Desalination and Water Treatment
www.deswater.com

doi: 10.5004/dwt.2023.29984

312 (2023) 218–233
November

Screening of various hybrid composite materials for removal of extremely toxic acid yellow dye from wastewater

Rabia Shaheen[a], Muhammad Asif Hanif[a,*], Shaukat Ali[a], Rashad Waseem Khan Qadri[b]

[a]*Department of Chemistry, University of Agriculture Faisalabad, 38040 Pakistan, emails: drmuhammadasifhanif@gmail.com (M.A. Hanif), rabiashaheen951@gmail.com (R. Shaheen), shaukatcolourist@yahoo.com (S. Ali)*
[b]*Institute of Horticultural Sciences, University of Agriculture Faisalabad, 38040 Pakistan, email: waseemrana_83pk@yahoo.com*

Received 7 June 2023; Accepted 19 September 2023

ABSTRACT

About 40,000 synthetic pigments and dyes are consumed in different industries throughout the world that severely contaminate water sources. The present study has been undertaken to remove extremely toxic and hazardous acid yellow dye from water. In total seven hybrid nanocomposites were prepared by mixing various materials with calcinized white stone powder (CWSP) and screened out for their dye removal efficiencies. The functional groups involved in the dye adsorption using 2% Cu/TiO_2 composite with calcinized white stone powder were Si–O, –CO and –OH. Scanning electron microscopy micrographs of 2% Cu/TiO_2 composite with calcinized white stone powder show that it has nano-granular structure as compared to other materials. The presence of distinctive and sharp peaks in X-ray diffraction indicated the crystalline nature of white stone powder, CWSP and 2% Cu/TiO_2-CWSP composite. The zeta potential measurements (−22.4 mV) of calcinized white stone powder indicate that these have anionic nature. The overall acid dye removal efficacy of various hybrid nanocomposites was in the following order: Cu/TiO_2-CWSP composite > Li/TiO_2-CWSP composite > CaO-Fe_3O_4-CWSP composite > CaO-Fe_2O_3-CWSP composite > $FeSnO_4$-CWSP composite, FeCdO-CWSP composite > Na_2SiO_3-CWSP composite. It is important to note that adsorbents have shown good adsorption at 30°C and 40°C. The optimized conditions for maximum removal of dye were pH 7, dose 0.05 g/L, initial concentration 40 mg/L and temperature 40°C. Almost 99.19% of acid yellow dye was removed by Cu/TiO_2-CWSP composite under optimized conditions.

Keywords: Water treatment; Acid yellow dye; Composite; Adsorption; Photocatalysis

1. Introduction

Acid dyes are anionic and applied at low pH values. Textile dyes including acid dyes are highly toxic, potentially carcinogenic, and have been linked to a variety of human and animal diseases [1,2]. Acid yellow dye is potentially harmful to human health and the environment. Acid yellow dye is one of the most used dyes and utilized in textile, personal care, cleaning materials and food industries [3]. Acid yellow dye is associated with risk of serious damage to eyes, impaired fertility, irritation to respiratory system and skin. It is extremely harmful to aquatic organisms, may cause long-term adverse effects in the aquatic environment [4]. The presence of this dye in water reduces penetration of sunlight into water sources and severely affects life present in aquatic systems. It also affects biochemical and physiological body mechanisms such as osmoregulation, mortality, respiration, and even reproduction. During the reduction of intermediates of dyes, the highly mutagenic or carcinogenic compounds are formed, having detrimental effects on aquatic life and microorganisms [5]. When humans use such polluted water, a number of detrimental health effects

* Corresponding author.

have been observed like, tissue necrosis, allergic reactions, breathing problems, immune suppression, disorders of the nervous system, infections related to eyes and skin, and behavioral problems.

Various techniques have been investigated for removing dye, including adsorption [6], electrochemical oxidation [7], chemical methods [8], biological methods [9], coagulation [10] and membrane separation [11]. Every technology, however, has advantages and disadvantages [2,5,12–15]. The main disadvantage of utilizing oxidation methods is that they might produce harmful byproducts in wastewater, from even biodegradable colors, which makes it difficult to remove pollutants completely. Frequently used chemical oxidation processes such as coagulation–flocculation and use of chlorine are slow and need reactive species that are hazardous to transport and store. Advanced oxidation processes like ozonation, photo Fenton, and photo catalyst are expensive and uneconomical [16]. Chemiocoagulation causes pollution due to the formation of colloids in polluted water [17].

Nanomaterials are efficient as adsorbents because of their low temperature modification, large surface area, short intraparticle diffusion distance, many sorption sites, surface chemistry, and variable pore size [18]. The characteristics and efficiency of nanoadsorbents are also influenced by their shape and morphology. The delicate balance between elastic deformation, surface area, and energy from polar charges, results in a variety of morphologies. The morphology besides the composition and surface area affected the behavior of nanoadsorbents towards the toxic materials [19,20]. Because of their chemical and physical properties, they are used as adsorbents more frequently than typical adsorbents. Moreover, chemical, physical and material properties are extremely affected by intrinsic compositions, external functionalization of nanoadsorbents, innate surface properties, and apparent sizes [21]. Wherever, the nature and allocation of active sites on nanoadsorbents surface, as well as the number and types of functional groups in nanoadsorbents, result in transitions of their properties and behavior, such as the high surface area, location of most atoms on surface, high chemical activity, high surface binding energy and high adsorptive capacity [22]. A raw substance, the marble stone is mainly comprised of calcite ($CaCO_3$), and dolomite [$(CO_3)_2$(CaMg)], that are based on carbonate material that exhibit very efficient removal capacities for dyes. According to an estimation, the marble waste production is around 6 million tonnes per year [23]. This marble waste causes pollution, so the use of marble waste in a productive way not only causes reduction in pollution but it is also economically favorable.

The present study has been undertaken to remove acid yellow dye using adsorption process by utilizing waste stones powders. In addition, hybrid composite materials were also studied for efficient dye removal. Cu/TiO_2 and Li/TiO_2 were prepared by doping of Cu and Li, respectively with TiO_2. Both Cu/TiO_2 and Li/TiO_2 were highly active photocatalysts and incorporated in the composite forms to optimize their photocatalytic and adsorption abilities in the hybrid form. CaO-Fe_2O_3, CaO-Fe_3O_4, $FeSnO_4$, and FeCdO are magnetically active compounds, and their hybrid forms were prepared with calcinized white stone. Sodium metasilicate (Na_2SiO_3) structure consists of layers containing SiO_4 tetrahedra and SiO_6 octahedra has high purifying and pH buffering abilities. The novelty of the study lies in the fact that the first-time adsorption process was applied in combination with various active materials including photocatalysts, magnetic materials and purifiers. Resultantly, two benefits were obtained, firstly, higher reduction in the acid yellow dye color was attained and secondly, the dye removal time has been reduced from 240 to 60 min. Finally, the effect of various process parameters including pH, dose, initial concentration, time and temperature was optimized and materials with high uptake capacities were characterized using advanced analytical techniques.

2. Materials and methods

2.1. Reagents/chemicals

All the chemicals used during the present study were of high purity and of analytical grade purchased from Sigma-Aldrich (USA). The used chemicals were including HCl, NaOH, $CuSO_4$, TiO_2, Na_2SiO_3, CaO, Fe_2O_3, Fe_3O_4, SnO_4, CdO.

2.2. Determination of maximum wavelengths of dye

Acid yellow 50 ppm solution was prepared, and wavelengths were scanned from 330 to 1,000 nm using UV-Visible spectrophotometer in order to determine their maximum absorption wavelengths.

2.3. Preparation of adsorbent materials

Abundantly available waste materials in powdered form white stone were used as adsorbent in the present study. The waste stones fine granules were washed with distilled water to remove dust and other contaminating materials. After washing these materials were dried at 70°C. The dried materials were grinded to fine powder form by using pestle and mortar. This material was calcinized in furnace at 700°C for 4 h to produced calcinized form.

2.4. Preparation of composites

To prepare Cu impregnated TiO_2 nano material, suspended 10 g of TiO_2 nanoform in 20 mL of distilled water at room temperature by constant slow stirring. The desired amount of cupric sulphate (for example 0.1 g for 1% doping) was added dropwise into TiO_2 suspension and mixture was stirred for 30 min magnetically. The obtained slurry was dried in an electric oven at 60°C till complete dryness. For calcination, the dried powder was heated at 450°C for 2 h. By using same procedure Cu impregnated TiO_2 nanoparticles of 0.5%–2.5% were prepared [24]. To prepare Li impregnated TiO_2 nano material, suspended 10 g of TiO_2 nanoform in 20 mL of distilled water at room temperature by constant slow stirring. The desired amount of $LiNO_3$ (for example 0.1 g for 1% doping) was added dropwise into TiO_2 suspension and mixture was stirred for 4 h magnetically. The obtained slurry was dried in an electric oven at 120°C till complete dryness. For calcination, the dried powder was heated at 600°C for 2h [24,25]. To prepare CaO-Fe_3O_4 (nano-magnetic material), added calcium nitrate (0.05 g) in 100 mL deionized distilled

water, then placed this mixture on magnetic stirrer and added 3.5 g of Fe_3O_4. The mixing was continued at 1,500 rpm for 10 min and then solution was dispersed at ultrasonic bath for 15 min. Then 100 mL of 2 M NaOH solution was added dropwise under constant stirring at 1,500 rpm until pH reached 12. The suspension was mechanically stirred overnight at 1,500 rpm. After that solution was filtered and precipitates were washed with excess quantity of distilled water obtained pH 7. The precipitates were heated at 80°C to complete dryness. After grinding to fine powder, the materials was subjected to calcination process at 550°C for 1 h in an electric furnace [26]. CaO-Fe_2O_3 (nano-magnetic material) was also prepared using above procedure just by replacing Fe_3O_4 with Fe_2O_3 [27]. FeCdO, and FeSnO (nano-magnetic material), were prepared through co-precipitation of $SnCl_2$ (0.5 mol/L) and $CdCl_2$ (0.5 mol/L) solution using $FeCl_3$ in an alkaline. The obtained dark precipitates were washed out using distilled water and the sediments were treated with HNO_3 (1 mol/L) and finally washed with distilled water. The obtained dark precipitates were filtered using Whatman filter paper No. 1. The precipitates were dried at 100°C in an electric oven for 2 h to completely remove moisture. The prepared FeCdO, and FeSnO nanoparticles were heated for 4 h at 300°C for activation [28,29]. After activation, the obtained materials were final ground before preparing composite materials. Cu/TiO_2-CWSP composite, Li/TiO_2-CWSP composite, Na_2SiO_3-CWSP composite, CaO-Fe_2O_3-CWSP composite, CaO-Fe_3O_4-CWSP composite, $FeSnO_4$-CWSP composite, FeCdO-CWSP composite were prepared by mixing materials with calcinized white stone powder (CWSP) in 10:90 ratio.

2.5. Factors affecting the dye removal process

Deionized distilled water (DDW) was used to prepare all the solutions. All the experiments were triplicated. For studying hybrid composite materials containing photocatalysts, all the samples were processed under sunlight.

2.5.1. Effect of pH

To determine the effect of pH, 50 ppm solutions of acid yellow dye was maintained at 5, 6, 7, 8, and 9 pH. The pH of solutions was set using a 1 N solution of nitric acid and a 1 N solution of sodium hydroxide. The pH of solution was monitored using a pH meter. After maintaining the pH of solutions having 50 ppm initial dye concentrations, 0.005 g/10 mL of adsorbent or composite material was added. Both blank and sample solutions were shaken at 40°C at 200 rpm for 240 min. Blank solution was run for every pH. After completion of required time period, the solutions were removed from orbital shaker, filtered using syringe filter (0.45 μm) and the absorbance was measured using a UV-Visible spectrophotometer [30].

2.5.2. Effect of dose

To determine the effect of adsorbent/composite dose, 0.5, 1, 2, 3, and 4 g/L were weighed accurately on an analytical balance and then added to 50 ppm solutions of acid yellow dye. The sample solutions (10 mL) were taken in taken 15 mL falcon tubes and were shaken at 40°C at 200 rpm for 240 min. After completion of required time, the blank and sample solutions were removed from orbital shaker, filtered using syringe filter (0.45 μm) and the absorbance were measured using a UV-Visible spectrophotometer [20].

2.5.3. Effect of initial dye concentration

The stock solutions of 100 ppm were prepared of acid yellow dye. The solutions of 5, 10, 15, 25, and 50 mg/L were prepared from the stock solution by dilution method. The 10 mL of each of these ppm solutions were taken in flacon tube and 0.005 g of each adsorbent or composite were added to it. These tubes were shaken at 200 rpm at 40°C for 240 min. The purpose of shaking was to increase the contact or interaction between the functional groups of adsorbents and molecules of dye in the solution. After shaking these solutions were filtered with the help of a syringe filter and the readings (absorbance) were measured at λ_{max} of dye using UV-Visible spectrophotometer [31].

2.5.4. Effect of time and temperature

The effect of time and temperature was determined by performing experiments at the temperature of 30°C, 40°C, 50°C, 60°C, and 70°C for a contact time interval of 15, 30, 60, 120, and 240 min. The 50 ppm solutions of acid yellow dye were prepared. 10 mL solutions were taken in 15 mL capacity falcon tube and added 0.005 g of adsorbent or composite. The sample solutions were shaken at 200 rpm. At the end of each experiment, adsorbent or composite was separated using syringe filter (0.45 μm) and absorbance were determined using a UV-Visible spectrophotometer at the λ_{max} of dye. All experiments of varying time interval and temperature conducted by adopting procedure [31].

2.6. Adsorption isotherms

This isotherm describes how adsorbate interacts with the adsorbent and critical in optimizing adsorbent usage. Adsorption equilibrium studies are arranged to associate the concentration of adsorbate (C_e, mg/L) and adsorption capacity (q_e, mg/g) in liquid phase. Different isotherm models were applied to understand complex adsorption system in liquid phase including Langmuir, Freundlich, Dubinin–Radushkevich, Temkin, and Harkin–Jura isotherms [32].

2.7. Kinetic modelling

Pseudo-first and second-order kinetic models were fitted to experimental data to describe the kinetics of the dye removal process [33].

2.8. Characterization studies

Fourier-transform infrared (FTIR) spectra was obtained using Agilent Technologies (USA), FTIR spectrometer from 4,000 to 650 cm^{-1} [25,34]. The scanning electron microscopy (SEM) images of adsorbents and composites were generated using the Nova NanoSEM 450, FEI, Oregon, USA equipped with built in ETD and TLD [35]. The X-ray diffraction (XRD)

spectra were obtained by using Shimadzu Model XRD-6000 Power X-ray Diffractometer (Japan) using Cu-Kα radiation (40 kV and 30 mA) with wavelength (λ) of 1.5406 Å. Data were collected over a 2θ range from 15° to 70° with a step of 0.02° at speed 6°/min. The obtained diffraction peaks were compared with standard compounds described in the JCPDS (Joint Committee on the Powder Diffraction Standards) databank [26,36]. Malvern, Zetasizer Nano ZSP was used to measure the particle size (hydrodynamic diameter) and size distribution.

2.9. Statistical analysis

The one-way analysis of variance (ANOVA) was used to compare the means between the treatments and to determine whether any of treatment means was statistically significantly different from each other. The Tukey's honestly significant difference test (Tukey's HSD) was used describe ANOVA results and to test differences among sample means for significance [37].

3. Results and discussions

3.1. Characterization studies

3.1.1. FTIR analysis

FTIR is a spectroscopic technique, used to identify the fingerprints, and functional group in a particular sample [38]. Some common peaks found in the FTIR spectra (Fig. 1) of most materials are as follows. The absorption peaks between 950–920 cm^{-1} could be assigned to Si–O bond stretching [38]. The shoulder peak in the range of 776–725 cm^{-1} corresponds to the Al–O bond stretching [38]. The medium intensity sharp peak around 3,650–3,550 cm^{-1} is due to –OH bond stretching present in Si–OH and Al–OH. The broadness and the shoulder of the OH bands are generally due to the combinations of several OH groups, occurring in the alkali family feldspar group from which stones powder are belonged to [39]. The presences of above-described functional groups in the stones powders provides effective adsorption sites for dye contaminants [40]. It is clear from results that calcinized white stone powder has more absorption bands in FTIR spectra. This means it can offer more active sites for adsorption of dyes. The involvement of regenerated absorption sites can be confirmed from dye loaded spectra of calcinized white stone powder. A comparison between FTIR spectra of calcinized white stone powder and its composite with 2% Cu/TiO_2 shows that after preparing composite materials maximum changes found to occur in 1,300–900 cm^{-1} (Si–O stretching vibrations). Cu/TiO_2 also interacted with calcinized white stone powder absorption peaks in the region of 1,800–1,500 cm^{-1} (–CO stretching vibrations) and 3,900–3,500 cm^{-1} (–OH stretching region) as the vibrations frequencies of functional groups reduced. The functional groups involved in the dye adsorption using 2% Cu/TiO_2 composite with calcinized white stone powder were Si–O, –CO and –OH). The dye removal by 2% Cu/TiO_2 composite with calcinized white stone powder occurred through photocatalysis in addition to adsorption. FTIR spectra of 10% Li/TiO_2 composite with calcinized white stone powder did not produce any major change from 1,300–900 cm^{-1} (Si–O stretching vibrations). However, there was prominent change in the frequency of absorption peaks in the region of 1,800–1,500 cm^{-1} (–CO stretching vibrations) and 3,900–3,500 cm^{-1} (–OH stretching region). A sharp band near 3,700 cm^{-1} in 10% Li/TiO_2 composite with calcinized white stone powder is attributed to –OH stretching (Si–OH and Al–OH). FTIR spectra of sodium metal silicate/calcinized white stone powder composite show a significant change in absorption peaks in the region of 1,300–900 cm^{-1} (Si–O stretching vibrations) of dye loaded 10% Li/TiO_2 composite with calcinized white stone powder suggests involvement of Si–O group in dye removal. FTIR spectra of CaO-Fe_2O_3/calcinized white stone powder composite has shown a prominent absorption peak around 1,008 cm^{-1} due to Si–O stretching in silicates. The Si–O group of silicates was involved in dye removal. FTIR spectra of CaO·Fe_3O_4/calcinized white stone powder composite shows that incorporation of CaO·Fe_3O_4 into calcinized white stone powder to produce a composite material mainly produced changes in the absorption peaks in the region of 1,800–1,500 cm^{-1} (–CO stretching vibrations) and 3,900–3,500 cm^{-1} (–OH stretching region). A sharp band near 3,700 cm^{-1} in composite is attributed to –OH stretching (Si–OH and Al–OH). FTIR spectra of dye loaded samples confirms the involvement of Si–O stretching vibrations region (1,300–900 cm^{-1}) in the dye adsorption process. FTIR spectra of FeCdO/calcinized white stone powder composite and $FeSnO_4$/calcinized white stone powder composite shows the involvement of the regions in the range of 1,300–900 cm^{-1} (Si–O stretching vibrations), 1,800–1,500 cm^{-1} (–CO stretching vibrations) and 3,900–35,00 cm^{-1} (–OH stretching region) in dye removal.

3.1.2. SEM analysis

SEM using built in ETD and TLD were utilized to investigate the surface structure of composites. Fig. 2 shows the SEM micrographs produced for the adsorbents and composites. According to these micrographs, the white stone powder and CaO-Fe_2O_3 composite with calcinized white stone powder has an aggregate coarse morphology with a heterogeneous surface. Calcinized form of white stone powder has more porous structure than non-calcinized form. It has many pores with irregular forms, rough and uneven surfaces. These pores have a larger area of contact and easy pore diffusion during adsorption. There are also other cage-like chambers. The porosity and voids in the treated composite increased the surface area and distance between the adsorption sites. SEM micrographs of 2% Cu/TiO_2 composite with calcinized white stone powder show that it has nano-granular structure as compared other materials. This composite is particularly effective in acid yellow dye removal because of increased surface area, porosity, and voids, which provide additional locations for reaction to occur [41].

3.1.3. X-ray diffraction analysis

The XRD spectra of white stone powder, calcinized white stone powder and 2% Cu/TiO_2-calcinized white stone powder composite is shown in Fig. 3. The presence distinctive and sharp peaks indicated the crystalline nature of white stone powder, calcinized white stone powder and 2% Cu/TiO_2-calcinized white stone powder composite. The XRD

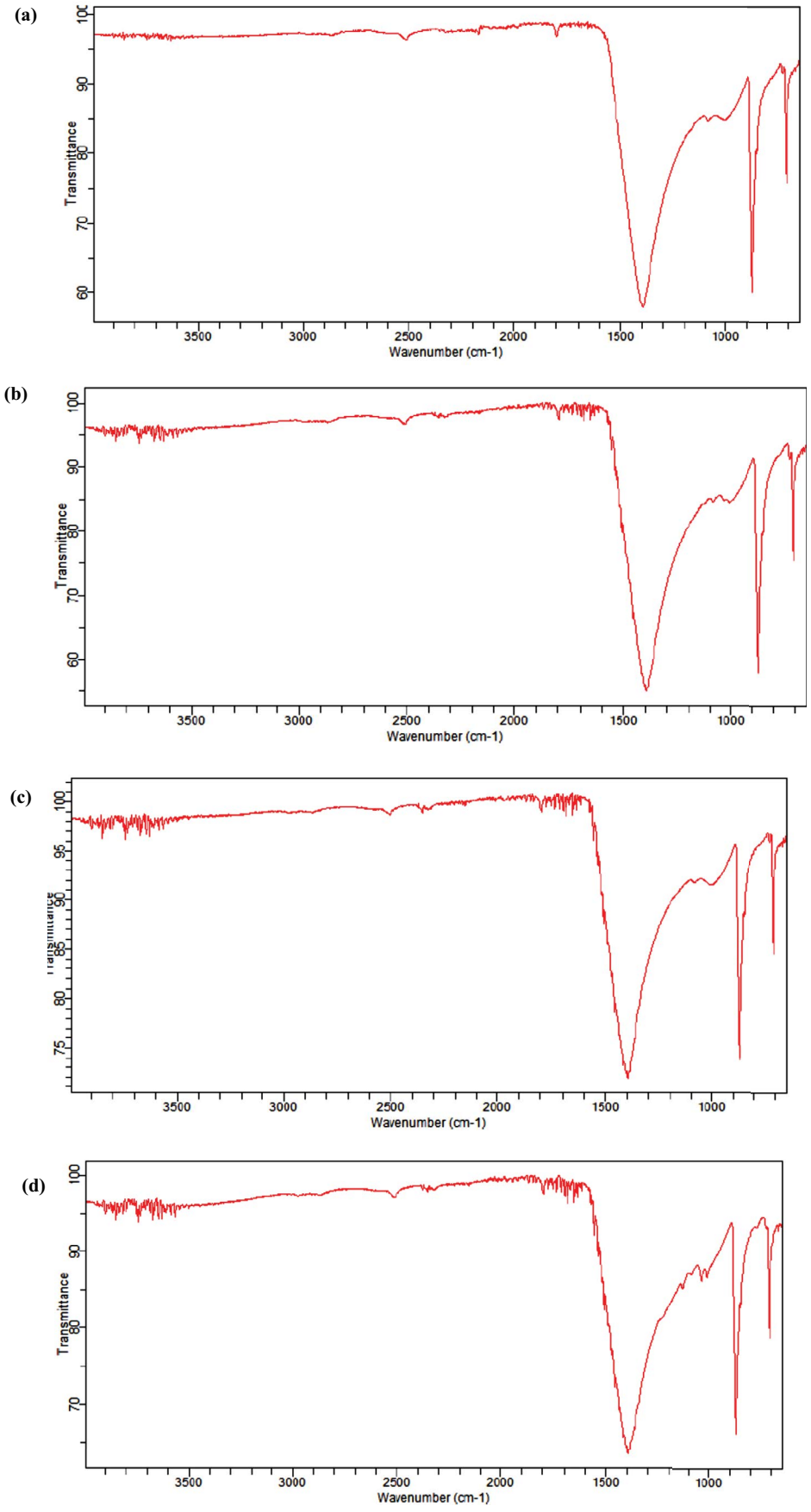

Fig. 1 (Continued)

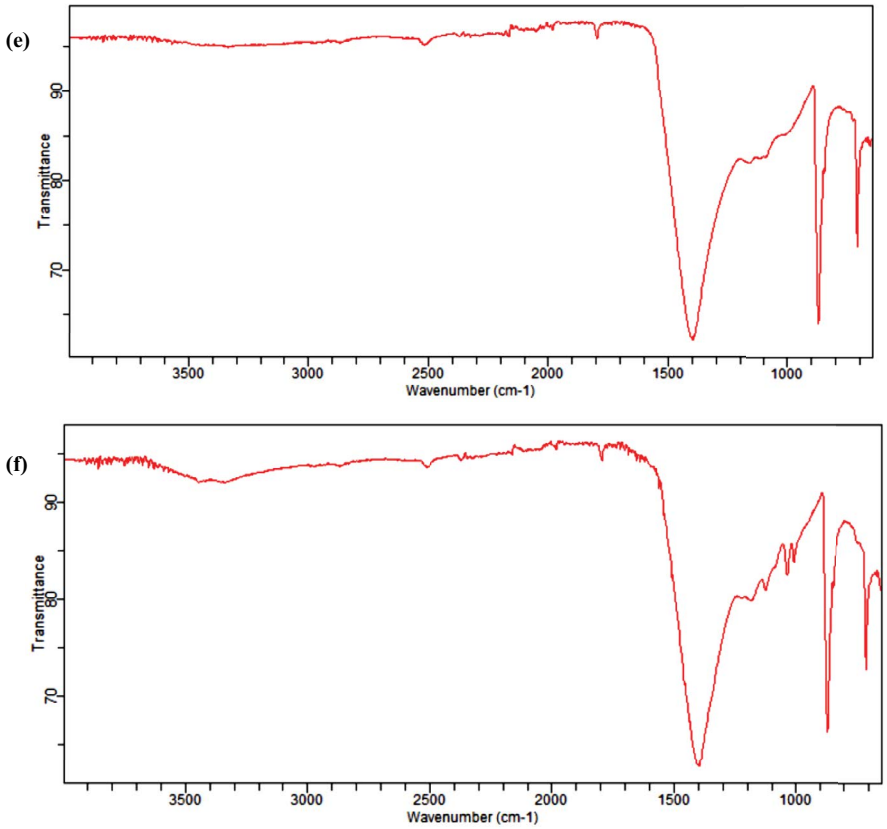

Fig. 1. Fourier-transform infrared spectra of (a) white stone powder, (b) white stone powder loaded with acid yellow dye, (c) calcinized white stone powder, (d) calcinized white stone powder loaded with acid yellow dye, (e) 2% Cu/TiO_2 composite with calcinized white stone powder, and (f) 2% Cu/TiO_2 composite with calcinized white stone powder loaded with acid yellow.

pattern of white stone powder, calcinized white stone powder and 2% Cu/TiO_2-calcinized white stone powder composite showed the characteristic pattern at 2θ values as 23.03°, 29.45°, 36.00°, 39.48°, 43.18°, 47.46°, 48.55°, and 51.06°; 23.06°, 29.42°, 30.93°, 33.56°, 39.41°, 43.20°, 47.59°, and 48.52°; and 29.34°, 30.93°, 35.99°, 39.42°, 41.11°, 43.21°, 48.53°, and 64.50°, respectively. These characteristic peaks clearly show that calcination has produced significant changes in white stone powder. The XRD pattern of white stone powder, calcinized white stone powder and 2% Cu/TiO_2-calcinized white stone powder composite showed the characteristic pattern at 2θ values as 23.03°, 29.45°, 36.00°, 39.48°, 43.18°, 47.46°, 48.55°, and 51.06°; 23.06°, 29.42°, 30.93°, 33.56°, 39.41°, 43.20°, 47.59°, and 48.52°; and 29.34°, 30.93°, 35.99°, 39.42°, 41.11°, 43.21°, 48.53°, and 64.50°, respectively. These characteristic peaks clearly show that calcination has produced significant changes in white stone powder [42–44]. The XRD patterns were thoroughly examined for calcium carbonate nanoparticles. In Fig. 3a, the XRD patterns of $CaCO_3$ are presented, unequivocally confirming the presence of a rhombohedral structure with the space group denoted as (R-3c). Notably, the discernible peaks in the XRD pattern correspond to specific Miller indices, including (012), (104), (006), (110), (113), (202), (018), (116), (211), (122), (214), and (300), aligning remarkably well with the JCPDS card number 01-086-2334, further affirming the rhombohedral nature of the structure. However, beyond the primary rhombohedral structure, it is evident that the introduction of copper and cobalt dopants led to the formation of some secondary phases. Specifically, the peaks labeled (002) and (131) can be attributed to the presence of CuO, as corroborated by the JCPDS File number 5-0661. It is worth noting that the symbol '&' designates the CuO phase in the XRD pattern.

3.1.4. Zeta sizer

Calcinized white stone powder was used to prepare all composite materials because of its higher uptake capacities. Zetasizer analysis of calcinized white stone powder is given in Fig. 4. There are two peaks in size distribution by intensity graph of calcinized white stone powder appeared. The peak 1 has 541.6 d.nm (size), 71.5% (intensity) and 174.0 (St. Dev.). The peak 2 has 180.9 d.nm (size), 28.5% (intensity) and 42.47 (St. Dev.). *Z*-average (d.nm) was 545.9. Zetasizer results of peak 1 show that particles of calcinized white stone powder have variable size and might be present in the form aggregates. SEM image of calcinized white stone powder also shows that it possesses a degree of heterogeneity. Zeta potential provides a measure of the particle's stability. The calcinized white stone powder has a zeta potential measurement (Fig. 4) of –22.4 mV with standard deviation of 5.50 mV and conductivity of 0.0525 mS/cm. If the zeta potential signal of nanoparticles is less than –30 mV or greater than +30 mV, these are considered as strongly

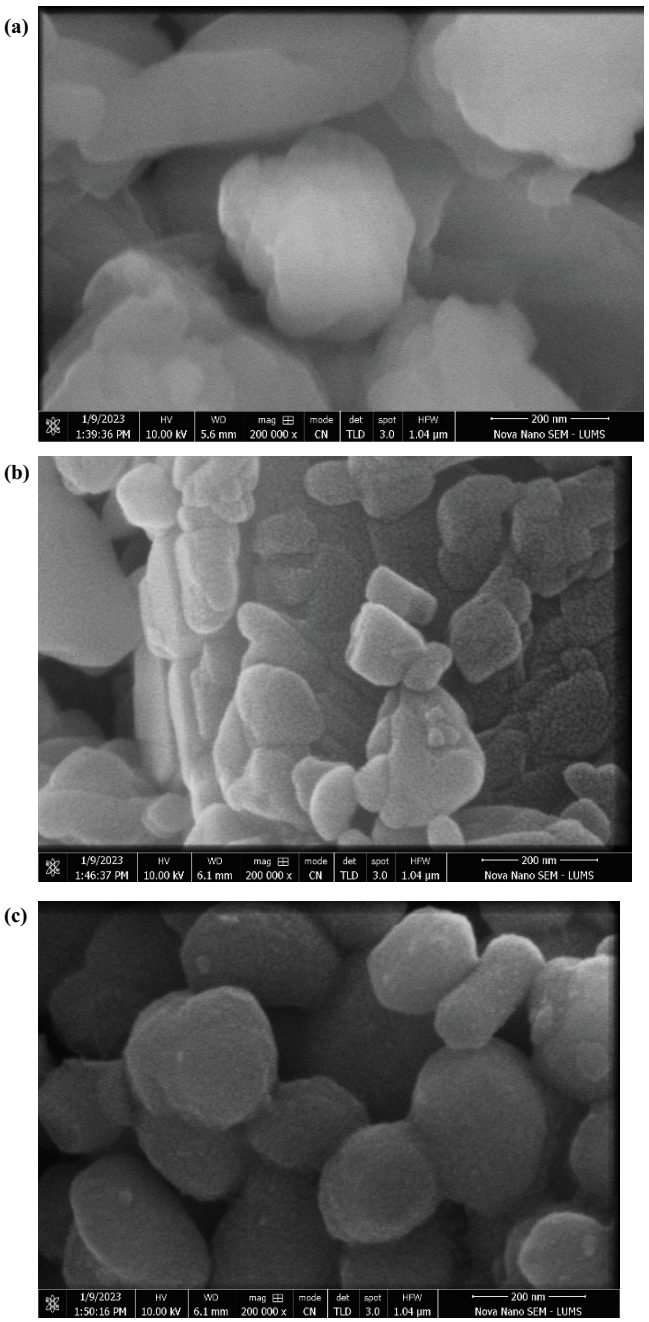

Fig. 2. Scanning electron micrographs of (a) white stone powder, (b) calcinized white stone powder, and (c) 2% Cu/TiO_2 composite with calcinized white stone powder.

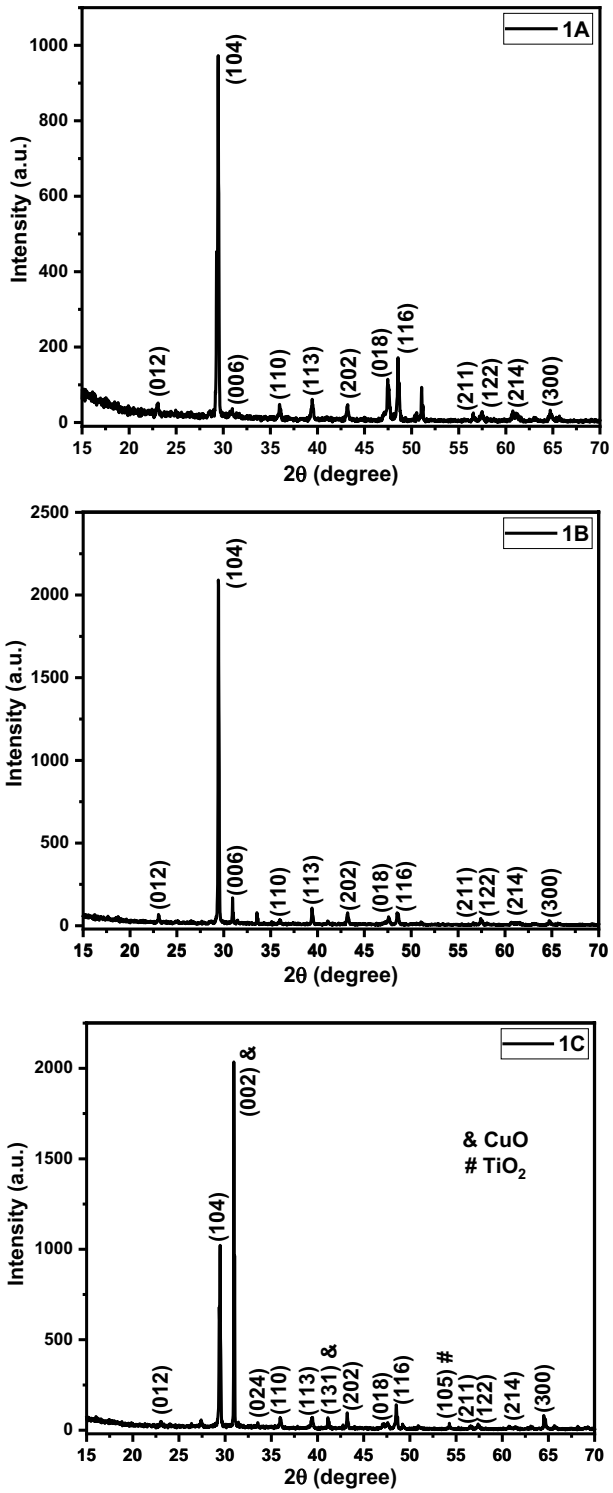

Fig. 3. X-ray diffraction analysis of (1A) white stone powder, (1B) calcinized white stone powder, and (1C) 2% Cu/TiO_2 and calcinized white stone powder composite.

anionic and strongly cationic, respectively. The zeta potential measurements (−22.4 mV) of calcinized white stone powder indicate that these have anionic nature.

3.1.5. Determination of λ_{max} and standard curves

The spectroscopic analysis are preferred because of accuracy, sensitivity, cost effectiveness, less waste of sample solution, and vastness [45]. In the present study, absorption wavelengths of acid yellow dye were scanned through 330 to 1,000 nm. λ_{max} of acid yellow dye was found to be 427 nm. The peak absorption at lambda wavelength (λ_{max}) is most important for studying material's properties like energy bandgap, sensitivity, electronic structure etc. λ_{max}, therefore,

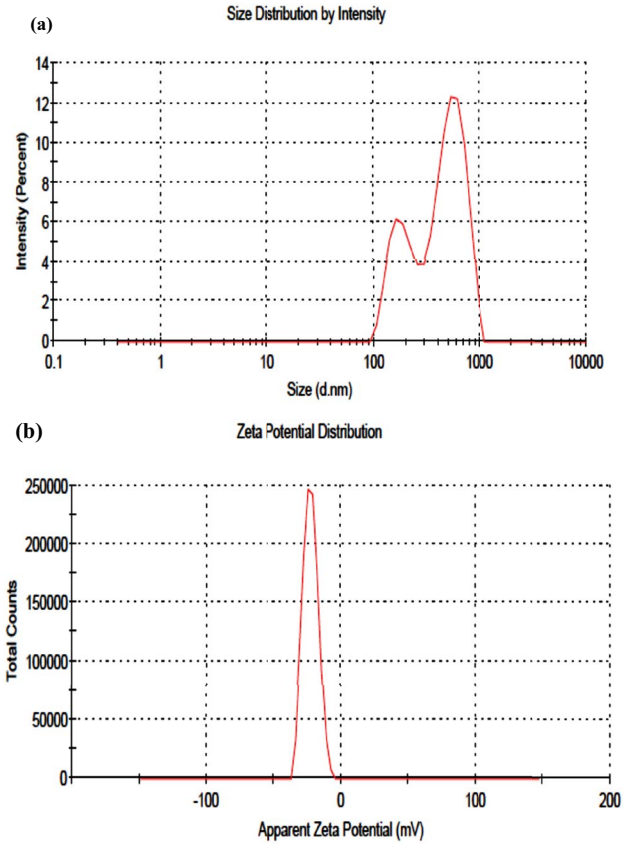

Fig. 4. Calcinized white stone powder (a) zetasizer analysis and (b) zeta potential distribution graph.

provides a clear hint of sample properties for identification and further analysis. In practice, unique λ_{max} values are determined by the use of pure samples [46]. The visible region is often preferred for distinguishing between different dyes samples. Spectroscopic analysis provides adequate speed required for water treatment studies [47]. Standard curves show the relationship between two variables or quantities. In absorption spectroscopy, the standard curves are drawn to find the relationship between absorbance and concentration. The concentration of unknown samples can be determined using standard curves. The standard curves for acid yellow dye were drawn using standards of 5, 10, 15, 25, 50, 75 and 100 ppm. The standard curve for acid yellow dye had a linear equation of $y = 0.0093x–0.003$ and R^2 of 0.9997. These results clearly suggested that there was a linear relationship between absorbance and concentration in the studied concentration range of 5–100 ppm of acid yellow dye.

3.2. Effect of pH

One of the most critical parameters affecting dye adsorption onto adsorbent is pH. Typically, pH is referred to as the "master variable". Because of its effect on the surface binding sites of the sorbent, the pH of the aqueous solution has a significant impact on dye sorptive absorption. Investigations have been done on how pH affects the elimination of dye from solutions. The degree of ionization of the adsorbate in the solution, the surface charge of the adsorbent, and the dissociation of different functional groups on the adsorbent's active sites are all significantly influenced by pH. The positively charged surface of the adsorbent and dye are electrostatically attracted to one another at low acidic to neutral pH values, which increases the dye absorption. However, when the pH above neutral rises, the positively charged adsorbent sites diminish and the adsorbent's surface becomes negatively charged. As a result of effective competition between OH– ions and dye ions at high pH, dye sorption is reduced. Additionally, a pH change has an impact on the adsorptive process by causing functional groups on the adsorbent surface to dissociate, which tends to modify the equilibrium properties of the adsorption process. White stone abundantly available waste material in powdered form was used in the present study. This material was calcinized in furnace at high temperatures to produce calcinized forms. On calcination various volatile materials and adsorbed gases are released thus resulting in the increase of adsorption sites and adsorption capacities [48].

The effect of pH (5, 6, 7, 8, 9 and 10) on acid yellow dye adsorption is shown in Fig. 5a. Two things were concluded from the results obtained. Calcinized form of material had shown better dye adsorption than its parent form. Secondly, dye adsorption was highest at neutral pH. The surface of the adsorbents and dye exhibited a strong electrostatic interaction at pH 7.0 in the present study. The number of negatively charged sites rises and the number of positively charged sites falls as the pH of the system rises. Due to electrostatic repulsion, a negatively charged surface site on the adsorbent does not encourage the adsorption of dye anions. Additionally, the existence of extra ions that compete with the dye anions for adsorption sites is the cause of the decreased dye adsorption at alkaline pH. According to the literature, at lower pH, the surface charge may become positively charged, leading (H^+) ions to compete efficiently with dye cations, resulting in a decrease in the quantity of dye adsorbed. At higher pH levels, the adsorbent materials may become negatively charged, enhancing the positively charged dye cations via electrostatic forces of attraction. Other authors explain this occurrence in the following ways: When dyes are dissolved in water, they emit positively charged ions. Thus, in an acidic media, the positively charged surface of the sorbent tends to impede cationic sorbate species adsorption. When the pH of the dye solution rises, the surface tends to acquire a negative charge, resulting in enhanced dye adsorption due to greater electrostatic interaction between positively charged sorbate and negatively charged sorbent [49].

3.3. Effect of adsorbent dose

The adsorption is a partitioning process of the adsorbate between the adsorbent and the fluid phase. An equilibrium distribution is reached, if the fluid and solid are placed in contact for a long time, and this equilibrium can be described quantitatively. It was observed that as the dose of adsorbent was increased, the efficacy of color removal improved. The nanocomposite dosage is critical in the absorption process since it impacts the nanocomposite's ability to absorb the dye. The efficiency of color removal improves as the mixture dosage is increased [50]. It is because the surface area

and active sites accessible for adsorption have increased. As a result, using a small amount of adsorbent with the same dye removal efficacy as a big amount of adsorbent is not advantageous in terms of cost and sludge output [51]. The effect of adsorbent dosage is shown in Fig. 5b. It can be observed from the results that higher uptake capacity can be obtained at lower adsorbent doses. The highest uptake capacity of acid yellow dye for white stone and calcinized white stone was obtained at 0.005 g/10 mL (0.5 g/L). On increasing dose from 0.005 g/10 mL to 0.04 g/10 mL, agglomeration of adsorbent molecules and fall in the inter-cellular space resulted in reduction in uptake capacity at higher doses [52].

3.4. Effect of initial concentration

The direct relationship between the dye concentration and the available binding sites on an adsorbent surface determines how the initial dye concentration will affect the surface. The removal of toxic dye acid yellow using white stone, and calcinized white stone were studied by varying initial dye concentration from 5 to 50 mg/L (Fig. 5c). From the results obtained, it can be seen clearly that acid yellow dye adsorption capacity of all adsorbents was high in the studied concentrations range. Calcinized form of adsorbent have shown better dye adsorption abilities than non-calcinized forms. The highest acid yellow adsorption was shown by calcinized white stone. The dye uptake capacity (mg/g) of calcinized white stone was 9.78, 19.35, 28.48, 47.18, and 93.93 mg/g for acid yellow concentrations (mg/L) of 5, 10, 15, 25, and 50 mg/L, respectively. The dye percentage removal (%) of calcinized white stone was 97.83%, 95.70%, 94.93%, 94.35%, and 93.71% for acid yellow dye concentrations (mg/L) of 5, 10, 15, 25, and 50 mg/L, respectively. The percentage removal of dye was high at lower concentrations, and it decreased at higher concentration for most of adsorbents used. With an increase in initial dye concentration, the percentage of dye removal often declines, which may be caused by the saturation of adsorption sites on the adhesive surface. When the initial dye concentration is low, there will be open active sites on the adsorbent surface, and as the initial dye concentration rises, the active sites needed for dye molecule adsorption will vanish. The strong driving force for mass at a high initial dye concentration may be the reason for the increased loading capacity of the absorbent that will result from an increase in the initial dye concentration. In other words, with larger starting dye concentrations, the residual concentration of dye molecules will be higher. Low initial dye molecule concentrations result in a low initial dye molecule to accessible adsorption site ratio, which makes fractional adsorption independent of initial concentration [53]. The percentage of dye removed, and quantity of dye (g/mg) adsorbed are significantly influenced by the initial concentration of the dye. Dye removal

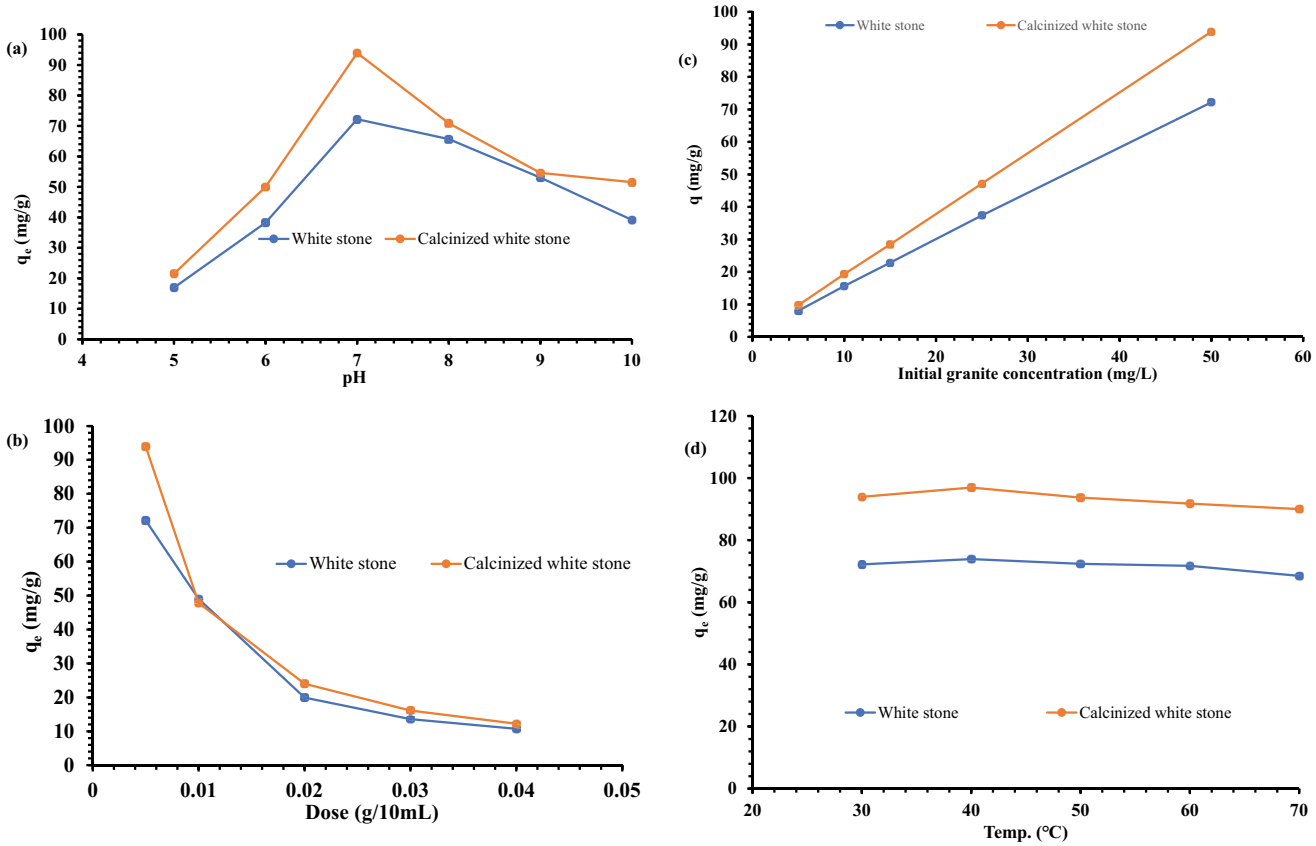

Fig. 5. Effect of (a) pH, (b) adsorbent dose, (c) initial dye concentration, and (d) temperature on acid yellow adsorption potential of various adsorbents.

efficiency is decreased when all the adsorption sites are occupied due to increased initial dye concentration. Increase in the contact time increases the amount of dye adsorbed regardless of the initial concentration of the dye used. All the resistances during transformation of dye from solution to adsorbent is overcome with the help of driving forces offered by the initial dye concentrations [54]. Furthermore, as the driving force of mass transfer between adsorbent and solution, the initial dye concentration is crucial. The high active sites on the composite interface and the low dye concentration in the solution resulted in a high sorption efficiency at low dye content. The ratio of active sites to dye molecules decreases as dye concentration in the solution increases, resulting in a decrease in sorption efficiency [50].

3.5. Isothermal adsorption modelling

Adsorption isotherms are useful for explaining how adsorbed species molecules or ions react with surface adsorption sites. As a result, correlation of equilibrium data using a mathematical or experimental equation is critical for adsorption interpretation and prediction [3]. Adsorption mechanisms are equations that represent the connection between the amount of the substance adsorbed by the adsorbent and the concentration of the solute in the liquid phase. They are crucial in the design of an adsorption process because they define how an adsorbed species interacts with an adsorbent. To characterize the connection between isotherms at equilibrium, several steady state models have been proposed. Langmuir, Freundlich, Temkin, and Dubinin–Radushkevich are commonly used to predict adsorption mechanisms. Adsorption isotherms are useful models for describing adsorption behavior in solid–liquid adsorption systems. When the adsorption process approaches equilibrium, the adsorption isotherm may show how dye molecules are distributed across the solid and liquid phases [22]. The close agreement between experimental uptake capacity and calculated uptake capacities and high values of linear regression coefficient (R^2) (Table 1) shows that the best fitted model for the adsorption of acid yellow dye to various adsorbents was Freundlich adsorption isotherm (Table 1). Freundlich adsorption isotherm states that the concentration of the solute absorbed onto the surface of the solid and the concentration of solute in the liquid phase have an empirical connection. The linearized forms of the Freundlich adsorption equations are applicable to liquid–solid adsorption equilibria. Since this connection is solely empirical, adsorption behavior should only be correctly suited by isotherms that have a theoretical foundation [55].

3.6. Effect of contact time at different solution temperatures

An immediately recognizable contaminant is dye, a component that is widely used in the textile, pulp, plastic, food, and cosmetics sectors. Environmental managers are presently facing a serious issue with decolorizing wastewater from textile and other industries. Because of the presence of aromatic hydrocarbons, metals, chlorides, and other substances in dyes, these substances may dramatically impact the photosynthetic activity of aquatic life. Numerous industrial colors are resistant to aerobic and are durable to light and oxidation. One of the most important aspects in the batch adsorption process is contact time.

Effect of contact time was studied at various temperatures including 30°C, 40°C, 50°C, 60°C and 70°C for the removal of toxic dye acid yellow using white stone and

Table 1
Adsorption models for acid yellow

Isothermal model		White stone powder	Calcinized white stone powder
Langmuir isotherm	R^2	0.8752	0.6653
	Q_{Cal}	204.08	169.49
	K_L	0.0373	0.3296
Freundlich isotherm	R^2	0.9996	0.9797
	Q_{Cal}	71.76	81.354
	K_f	8.05	38.21
	$1/n$	0.8284	0.6698
Dubinin–Radushkevich isotherm	R^2	0.7371	0.7326
	Q_{Cal}	39.527	50.703
	β	6.00E-07	5.00E-08
Temkin isotherm model	R^2	0.8999	0.8948
	A_t	0.247	0.197
	Q_{Cal}	35.7505	17.428
	B	28.77	36.61
Harkin–Jura isotherm model	R^2	0.749	0.8419
	A	80	140.845
	Q_{Cal}	19.1171	24.2918
	B	0.928	0.253
Experimental uptake capacity (mg/g)	Q_{Exp}	72.19	93.93

calcinized white stone and obtained results are shown in Fig. 5d. The results obtained clearly demonstrated that adsorption process can be divided into two phases. An initial phase during first 60 min during which adsorption of dye was very fast followed by a slower phase till equilibrium time of 240 min. The appropriate adsorption time for acid yellow dye was 240 min.

Regardless of the dye's starting concentration, a longer contact period increases the quantity of dye that is adsorbed. The driving forces provided by the initial concentrations of dye are used to overcome all resistances during the dye's transition from solution to adsorbent [54]. The initial amount of dye is also critical because it serves as the catalyst for mass transfer between the adsorbent and solution. A higher adsorption efficiency at low dye content was achieved due to the high active sites on the composite surface and the low concentration of dye in the solution. As the concentration of dye in the solution rises, the ratio of catalyst surface to dye molecules declines, which lowers the sorption efficiency [50]. The adsorption rate grew fast at first, and the optimum removal efficiency was obtained in around 240 min. Further increase in contact time did not show significant change in equilibrium concentration; that is, the adsorption phase reached equilibrium.

The change in temperature significantly affect the process in two ways; change in temperature before and after the attainment of equilibrium affect the rate at which the dye gets adsorb. More precisely, adsorption equilibrium is affected by the temperature equilibrium for specific adsorbate. Dye adsorption can be any of these processes, that is, endothermic, and exothermic. Increase in temperature increases the adsorption for endothermic adsorption reaction and decrease in temperature enhance the capacity of adsorption for exothermic adsorption reaction. The adsorption of acid yellow dye using white stone, and calcinized white stone was studied in the temperature range from 30°C to 70°C. Acid yellow dye adsorption was increased on increasing temperature from 30°C to 40°C and then decreased on increasing temperature 40°C to 70°C. It is important to note that adsorbents have shown good adsorption at 30°C and 40°C. This suggested that adsorption process can be conducted at ambient conditions without any requirement of elevated temperatures [54].

3.7. Kinetic modelling

Pseudo-first-order and pseudo-second-order kinetic models were applied to the removal of toxic dye acid yellow using white stone and calcinized white stone at various time intervals on temperatures 30°C to 70°C. Kinetic data or equilibria data is critical for understanding the mechanism of adsorption processes. It was obtained during the experimental work through kinetic models (Table 2). The calculated parameters for pseudo-first-order and pseudo-second-order kinetic models for acid yellow dye is shown in Table 2. The results obtained clearly demonstrated that pseudo-second-order better fitted to data.

The slope of the presented graph connecting time (t) and $\log(q_e-q)$ were used to compute the values of q_e and $K_{1,ads}$. The disparity between the practical and estimated q values, as well as the correlation coefficient R^2 values, indicated that acid yellow dye was not obeying pseudo-first-order kinetics. The intercept and slope of the presented graphs connecting time (t) and t/q were used to compute the values of q_e and $K_{2,ads}$. Pseudo-second-order kinetics is based on the idea that the rate limiting step is chemisorption, which

Table 2
Kinetic models for acid yellow at different temperatures

Adsorbents	Pseudo-first-order kinetics				Pseudo-second-order kinetics		
	q_e (mg/g) Cal	$K_{1,ads}$	R^2	q (mg/g) Exp	q_e (mg/g)	$K_{2,ads}$	R^2
			30°C				
White stone	38.9941	0.0276	0.9171	72.20	76.3358	0.00116	0.9984
Calcinized white stone	41.2097	0.01335	0.9972	93.93	99.0099	0.000679	0.9979
			40°C				
White stone	40.8319	0.0343	0.9309	73.93	77.5193	0.0011282	0.9988
Calcinized white stone	41.8793	0.0165	0.9809	96.98	102.04	0.000655	0.9974
			50°C				
White stone	42.4619	0.03247	0.945	72.41	76.3358	0.001175	0.9984
Calcinized white stone	40.6443	0.0128	0.9985	93.72	98.0392	0.000701	0.9979
			60°C				
White stone	39.4457	0.0278	0.9193	71.75	75.7575	0.001167	0.9984
Calcinized white stone	40.5508	0.0119	0.9998	91.76	96.1538	0.0007474	0.9983
			70°C				
White stone	49.545	0.0145	0.9496	68.49	76.3358	0.0004997	0.9991
Calcinized white stone	64.7142	0.00806	0.9775	90.02	103.0927	0.000225	0.9836

indicates the participation of valance electrons between the adsorbate and adsorbent via electron sharing or exchange. The adsorption capabilities (q_e) determined from the data were at their highest in this example. Furthermore, the correlation coefficient (R^2) was between 1 and 0.98, indicating that ($1 > R^2 > 0.98$). This meant that acid yellow dye followed the pseudo-second-order kinetics.

3.8. Screening of nanocomposites

The dye adsorption capacity of white stone powder increased on calcination. Therefore, calcinized white stone powder (CWSP) was used for preparation of various nanocomposites with Cu/TiO_2, Li/TiO_2, sodium metasilicate, CaO-Fe_2O_3, CaO-Fe_3O_4, $FeSnO_4$, and FeCdO. pH_{pzc} (point of zero charge) calcinized form of white stone powder was determined by the pH drift method [56]. The pH initial–pH final curve in Fig. 6 using the measured pH initial and pH final values. The pH_{pzc} was determined from intersection of the curves and the pH initial = pH final line showed that the pH_{pzc} was 7. The determination of PZC is imperative for the prediction of the functional groups ionization and their interaction with dyes species in solution [56]. In total seven nanocomposites were prepared and screened out for their dye removal efficiencies. Cu/TiO_2 and Li/TiO_2 were prepared by doping of Cu and Li, respectively with TiO_2. Both Cu/TiO_2 and Li/TiO_2 were highly active photocatalysts and incorporated in the composite forms to optimize their photocatalytic and adsorption abilities in the hybrid form. CaO-Fe_2O_3, CaO-Fe_3O_4, $FeSnO_4$, and FeCdO are magnetically active compounds, and their hybrid forms were prepared with calcinized white stone. Sodium metasilicate (Na_2SiO_3) structure consists of layers containing SiO_4 tetrahedra and SiO_6 octahedra has high purifying and pH buffering abilities. Cu/TiO_2-CWSP composite, Li/TiO_2-CWSP composite, Na_2SiO_3-CWSP composite, CaO-Fe_2O_3-CWSP composite, CaO-Fe_3O_4-CWSP composite, $FeSnO_4$-CWSP composite, FeCdO-CWSP composite were prepared by mixing materials with CWSP in 10:90

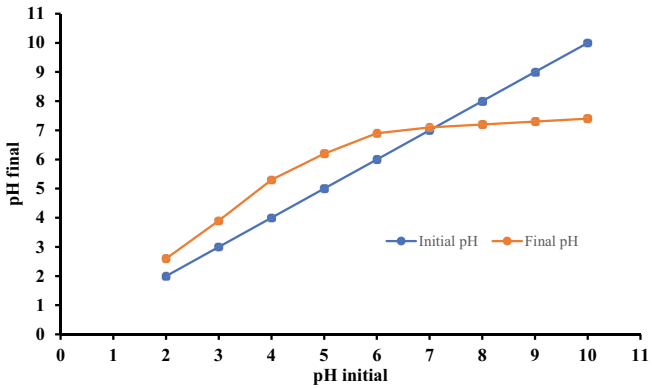

Fig. 6. pH_{pzc} of calcinized white stone powder.

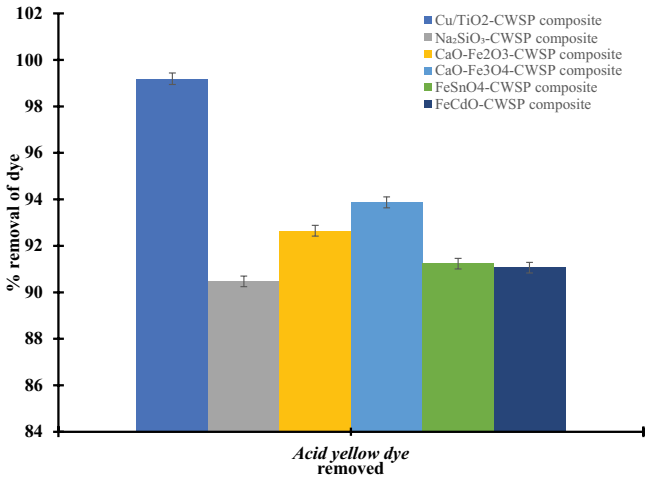

Fig. 7. Efficacy of various nanocomposites for dye removal.

Table 3
Comparison of various materials for acid yellow dye removal

Sr. No.	Material	Dye	% Removed	References
1	Cu/TiO_2-CWSP composite	Acid yellow	99.19	The present study
2	Activated bone char	Acid Yellow-17	91.43	[58]
3	Activated water hyacinth	Acid Yellow-17	92.26	[59]
4	H_2O_2/Fe^{2+}	Acid Yellow-17	89.00	[60]
5	*Typha angustifolia* L.	Acid Yellow-17	89.98	[61]
6	Chitin	Acid Yellow-25	95.00	[62]
7	Modified biochar derived from watermelon peels	Acid Yellow-17	96.00	[63]
8	Turmeric industrial waste activated carbon	Acid Yellow-17	98.00	[64]
9	*Moringa peregrina* seeds	Acid yellow	80.00	[65]
10	Activated rice husk	Acid Yellow-17	94.34	[66]
11	Fish scales	Acid Yellow-127	93.00	[67]
12	Reverse micelles	Acid Yellow-36	96.93	[68]
13	Kant Rita carbon sample	Acid Yellow RR	70.00	[69]
14	Fly ash mixtures with a sandy clay loam soil	Acid Yellow-7	53.00	[70]
15	Fly ash mixtures with a sandy clay loam soil	Acid Yellow-23	44.90	[70]

Table 4
Statistical analysis for acid yellow dye adsorption by various nanocomposites

Composite	Code
Cu/TiO_2-CWSP composite	A
Li/TiO_2-CWSP composite	B
Na_2SiO_3-CWSP composite	C
$CaO\text{-}Fe_2O_3$-CWSP composite	D
$CaO\text{-}Fe_3O_4$-CWSP composite	E
$FeSnO_4$-CWSP composite	F
FeCdO-CWSP composite	G

One-way analysis of variance

Source	Sum of squares SS	Degrees of freedom νν	Mean square MS	*F* statistic	*p*-value
Treatment	174.7842	6	29.1307	611,744.8198	1.1102e-16
Error	0.0007	14	0.0000		
Total	174.7849	20			

Tukey HSD results

Treatments pair	Tukey HSD *Q* statistic	Tukey HSD *p*-value	Tukey HSD inference
A vs. B	884.3496	0.0010053	** $p < 0.01$
A vs. C	2,187.8659	0.0010053	** $p < 0.01$
A vs. D	1,642.3636	0.0010053	** $p < 0.01$
A vs. E	1,335.3094	0.0010053	** $p < 0.01$
A vs. F	1,999.6174	0.0010053	** $p < 0.01$
A vs. G	2,043.1237	0.0010053	** $p < 0.01$
B vs. C	1,303.5163	0.0010053	** $p < 0.01$
B vs. D	758.0140	0.0010053	** $p < 0.01$
B vs. E	450.9597	0.0010053	** $p < 0.01$
B vs. F	1,115.2678	0.0010053	** $p < 0.01$
B vs. G	1,158.7741	0.0010053	** $p < 0.01$
C vs. D	545.5023	0.0010053	** $p < 0.01$
C vs. E	852.5565	0.0010053	** $p < 0.01$
C vs. F	188.2485	0.0010053	** $p < 0.01$
C vs. G	144.7422	0.0010053	** $p < 0.01$
D vs. E	307.0542	0.0010053	** $p < 0.01$
D vs. F	357.2538	0.0010053	** $p < 0.01$
D vs. G	400.7601	0.0010053	** $p < 0.01$
E vs. F	664.3080	0.0010053	** $p < 0.01$
E vs. G	707.8144	0.0010053	** $p < 0.01$
F vs. G	43.5063	0.0010053	** $p < 0.01$

ratio, respectively. The prepared composite was used at the dose of 0.5 g/L for a contact time up to 240 min to determine dye removal efficiencies (Fig. 7). A maximum dye removal was attained within 60 min. From the results obtained, it can be concluded that Cu/TiO_2-CWSP composite was more effective in removal of acid yellow dye in comparison to other nanocomposites. The overall acid dye removal efficacy of various nanocomposites was in the following order: Cu/TiO_2-CWSP composite > Li/TiO_2-CWSP composite > $CaO\text{-}Fe_3O_4$-CWSP composite > $CaO\text{-}Fe_2O_3$-CWSP composite > $FeSnO_4$-CWSP composite, FeCdO-CWSP composite > Na_2SiO_3-CWSP composite. A comparison of various materials including Cu/TiO_2-CWSP composite, activated bone char, activated water hyacinth, H_2O_2/Fe^{2+}, *Typha angustifolia* L. and chitin for acid yellow dye removal is given in Table 3. It is clear from comparative information given in the table that Cu/TiO_2-CWSP composite removed acid yellow dye in highest percentage (99.19%) than other materials.

3.9. Statistical analysis

The one-way ANOVA compares the means between the treatments and determines whether any of treatment means

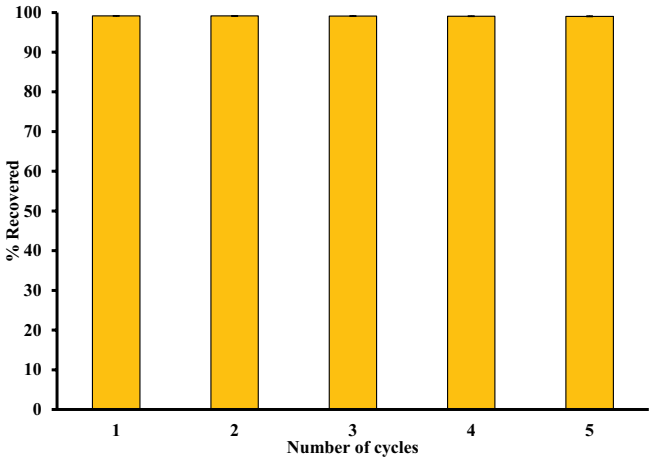

Fig. 8. Regeneration studies of composite material.

are statistically significantly different from each other. The Tukey's honestly significant difference test (Tukey's HSD) is used describe ANOVA results and to test differences among sample means for significance. The removal of acid yellow dye using Cu/TiO_2-CWSP composite, Li/TiO_2-CWSP composite, Na_2SiO_3-CWSP composite, CaO-Fe_2O_3-CWSP composite, CaO-Fe_3O_4-CWSP composite, $FeSnO_4$-CWSP composite, FeCdO-CWSP composite were tested using comparative statics including ANOVA and Tukey HSD test. The *p*-value given in ANOVA (Table 4) corresponding to the *F*-statistic of one-way ANOVA for all samples was lower than 0.05, suggesting that all treatments were significantly different. For Tukey HSD test, the *p*-value corresponding to the *F*-statistic of one-way ANOVA was lower than 0.01 which strongly suggested that all pairs of treatments were significantly different. Color coded results (red for insignificant, green for significant).

3.10. Regeneration of Cu/TiO_2-CWSP composite

The regeneration of acid yellow dye from Cu/TiO_2-CWSP composite was investigated using CH_3OH as an eluent for five consecutive cycles (Fig. 8). The amount of acid yellow dye present in CH_3OH was determined spectrophotometrically and the removal efficiency was determined after each cycle [57]. Cu/TiO_2-CWSP composite intermediate washing was done with excess amount of deionized distilled water before reusing in the adsorption studies. The distilled water used in the present study was deionized having a resistivity of 18.2 megohm and conductivity of 0.055 microsiemens. There was a very slight change in acid yellow uptake capacity of Cu/TiO_2-CWSP composite after each cycle which suggested that this material can be effectively used without any significant loss in the dye uptake capacity for up to five cycles.

4. Conclusions

The present study described the comparative abilities of various hybrid composite materials to remove acid yellow dye. These hybrid composite materials were comprised of calcinized white stone powder combined with various materials including photocatalysts (Cu/TiO_2, and Li/TiO_2), magnetically active compounds (CaO-Fe_2O_3, CaO-Fe_3O_4, $FeSnO_4$, and FeCdO) and purifier material Sodium metasilicate (Na_2SiO_3). Among these materials Cu/TiO_2 composite with calcinized white stone powder was found to have highest dye removal efficiency. The dye removal data was well described by Freundlich adsorption isotherm and pseudo-second-order kinetics. The functional groups involved in the dye adsorption using 2% Cu/TiO_2 composite with calcinized white stone powder were Si–O, –CO and –OH. The dye removal by 2% Cu/TiO_2 composite with calcinized white stone powder occurred through photocatalysis in addition to adsorption. SEM micrographs of 2% Cu/TiO_2 composite with calcinized white stone powder show that it has nano-granular structure as compared other materials. This composite is particularly effective in acid yellow dye removal because of increased surface area, porosity, and voids, which provide additional locations for reaction to occur.

Acknowledgments

Authors are thankful to NBL fellows for useful discussion during the present research which is part of PhD thesis of first author.

Data availability statement

The manuscript has no associated data.

Conflict of interest

The authors declare that they have no conflict of interest.

References

[1] A. Tariq, A. Mushtaq, Untreated wastewater reasons and causes: a review of most affected areas and cities, Int. J. Chem. Biochem. Sci., 23 (2023) 121–143.
[2] A. Choudhary, A. Mushtaq, From pollutant to valuable product: a novel reutilization strategy of wastewater, Int. J. Chem. Biochem. Sci., 23 (2023) 31–37.
[3] E. Adar, Removal of Acid Yellow 17 from textile wastewater by adsorption and heterogeneous persulfate oxidation, Int. J. Environ. Sci. Technol., 18 (2021) 483–498.
[4] J. Wang, R. Liu, P. Qin, Toxic interaction between Acid Yellow 23 and trypsin: spectroscopic methods coupled with molecular docking, J. Biochem. Mol. Toxicol., 26 (2012) 360–367.
[5] F. Asghar, A. Mushtaq, The future of nanomaterial in wastewater treatment: a review, Int. J. Chem. Biochem. Sci., 23 (2023) 150–157.
[6] S.-H. Kim, D.-S. Kim, H. Moradi, Y.-Y. Chang, J.-K. Yang, Highly porous biobased graphene-like carbon adsorbent for dye removal: preparation, adsorption mechanisms and optimization, J. Environ. Chem. Eng., 11 (2023) 109278, doi: 10.1016/j.jece.2023.109278.
[7] A.B. Isaev, N.S. Shabanov, A.G. Magomedova, P.V. Nidheesh, M.A. Oturan, Electrochemical oxidation of azo dyes in water: a review, Environ. Chem. Lett., 21 (2023) 2863–2911.
[8] C. Valli Nachiyar, A.D. Rakshi, S. Sandhya, N. Britlin Deva Jebasta, J. Nellore, Developments in treatment technologies of dye-containing effluent: a review, Case Stud. Chem. Environ. Eng., 7 (2023) 100339, doi: 10.1016/j.cscee.2023.100339.
[9] H.M. Solayman, Md.A. Hossen, A. Abd Aziz, N.Y. Yahya, L.K. Hon, S.L. Ching, M.U. Monir, K.-D. Zoh, Performance evaluation of dye wastewater treatment technologies: a review, J. Environ. Chem. Eng., 11 (2023) 109610, doi: 10.1016/j.jece.2023.109610.

[10] A. Hadadi, A. Imessaoudene, J.-C. Bollinger, A. Bouzaza, A. Amrane, H. Tahraoui, L. Mouni, Aleppo pine seeds (*Pinus halepensis* Mill.) as a promising novel green coagulant for the removal of Congo red dye: optimization via machine learning algorithm, J. Environ. Manage., 331 (2023) 117286, doi: 10.1016/j.jenvman.2023.117286.
[11] X. Zhao, X. Wang, Y. Lv, W. Zhao, Y. Dong, L. Wang, Sodium alginate intercalated 2D g-C_3N_4 membrane: efficient dye removal and photocatalytic self-cleaning, Sep. Purif. Technol., 320 (2023) 124177, doi: 10.1016/j.seppur.2023.124177.
[12] T. Fatima, A. Mushtaq, Efficacy and challenges of carbon-based nanomaterials in water treatment: a review, Int. J. Chem. Biochem. Sci., 23 (2023) 232–248.
[13] M.S. Hamada, R.A. Jabal, Doped (Ag) ZnO nanoparticles for removal of azo dyes from aqueous solutions, Int. J. Chem. Biochem. Sci., 21 (2022) 210–217.
[14] A. Javed, A. Mushtaq, A critical review of electrocoagulation and other electrochemical methods Int. J. Chem. Biochem. Sci., 23 (2023) 98–110.
[15] Z. Rehman, A. Mushtaq, Advancements in treatment of high-salinity wastewater: a critical, Int. J. Chem. Biochem. Sci., 23 (2023) 1–10.
[16] O. Can, M. Kobya, E. Demirbas, M. Bayramoglu, Treatment of the textile wastewater by combined electrocoagulation, Chemosphere, 62 (2006) 181–187.
[17] C.A. Basha, N. Bhadrinarayana, N. Anantharaman, K.M.S. Begum, Heavy metal removal from copper smelting effluent using electrochemical cylindrical flow reactor, J. Hazard. Mater., 152 (2008) 71–78.
[18] M.M. Khin, A.S. Nair, V.J. Babu, R. Murugan, S. Ramakrishna, A review on nanomaterials for environmental remediation, Energy Environ. Sci., 5 (2012) 8075–8109.
[19] M.A. Gatoo, S. Naseem, M.Y. Arfat, A. Mahmood Dar, K. Qasim, S. Zubair, Physicochemical properties of nanomaterials: implication in associated toxic manifestations, BioMed Res. Int., 2014 (2014) 498420, doi: 10.1155/2014/498420.
[20] Y. Chauhdary, M.A. Hanif, U. Rashid, I.A. Bhatti, H. Anwar, Y. Jamil, F.A. Alharthi, E.A. Kazerooni, Effective removal of reactive and direct dyes from colored wastewater using low-cost novel bentonite nanocomposites, Water, 14 (2022) 3604, doi: 10.3390/w14223604.
[21] M. Khajeh, S. Laurent, K. Dastafkan, Nanoadsorbents: classification, preparation, and applications (with emphasis on aqueous media), Chem. Rev., 113 (2013) 7728–7768.
[22] M.E. El-Sayed, A.F. Ahmed, O.A. Farghaly, M. Abd-Elmottaleb, T.A.S. Elnasr, M.A. Hassan, Preparation and using modified nanohydroxyapatite molecules for wastewater treatment, Water Conserv. Sci. Eng., 3 (2018) 331–337.
[23] A. Viswakarma, R.R. Singh, Utilization of marble slurry to enhance soil properties and protect environment, J. Environ. Res. Dev., 7 (2013) 1479–1483.
[24] A. De, S.S. Boxi, Application of Cu impregnated TiO_2 as a heterogeneous nanocatalyst for the production of biodiesel from palm oil, Fuel, 265 (2020) 117019, doi: 10.1016/j.fuel.2020.117019.
[25] M. Alsharifi, H. Znad, S. Hena, M. Ang, Biodiesel production from canola oil using novel Li/TiO_2 as a heterogeneous catalyst prepared via impregnation method, Renewable Energy, 114 (2017) 1077–1089.
[26] M.A. Ali, I.A. Al-Hydary, T.A. Al-Hattab, Nano-magnetic catalyst CaO-Fe_3O_4 for biodiesel production from date palm seed oil, Bull. Chem. React. Eng. Catal., 12 (2017) 460–468.
[27] M. Shi, P. Zhang, M. Fan, P. Jiang, Y. Dong, Influence of crystal of Fe_2O_3 in magnetism and activity of nanoparticle CaO@Fe_2O_3 for biodiesel production, Fuel, 197 (2017) 343–347.
[28] H.Q. ul Ain Sami, M.A. Hanif, U. Rashid, S. Nisar, I.A. Bhatti, S.L. Rokhum, T. Tsubota, A. Alsalme, Environmentally safe magnetic nanocatalyst for the production of biodiesel from *Pongamia pinnata* oil, Catalysts, 12 (2022) 1266, doi: 10.3390/catal12101266.
[29] M.B. Alves, F. Medeiros, M.H. Sousa, J.C. Rubim, P.A. Suarez, Cadmium and tin magnetic nanocatalysts useful for biodiesel production, J. Braz. Chem. Soc., 25 (2014) 2304–2313.
[30] M.A. Hanif, R. Nadeem, H.N. Bhatti, N.R. Ahmad, T.M. Ansari, Ni(II) biosorption by *Cassia fistula* (Golden Shower) biomass, J. Hazard. Mater., 139 (2007) 345–355.
[31] I. Javed, M.A. Hanif, U. Rashid, F. Nadeem, F.A. Alharthi, E.A. Kazerooni, Enhancing functionalities in nanocomposites for effective dye removal from wastewater: isothermal, kinetic and thermodynamic aspects, Water, 14 (2022) 2600, doi: 10.3390/w14172600.
[32] M. Amin, A. Alazba, M. Shafiq, Adsorptive removal of Reactive black 5 from wastewater using bentonite clay: isotherms, kinetics and thermodynamics, Sustainability, 7 (2015) 15302–15318.
[33] Y. Ho, G. McKay, D. Wase, C. Forster, Study of the sorption of divalent metal ions on to peat, Adsorpt. Sci. Technol., 18 (2000) 639–650.
[34] K.R. Borba, P.C. Spricigo, D.P. Aykas, M.C. Mitsuyuki, L.A. Colnago, M.D. Ferreira, Non-invasive quantification of vitamin C, citric acid, and sugar in 'Valência' oranges using infrared spectroscopies, J. Food Sci. Technol., 58 (2021) 731–738.
[35] B. Iqbal, M. Saleem, S.N. Arshad, J. Rashid, N. Hussain, M. Zaheer, One-pot synthesis of heterobimetallic metal–organic frameworks (MOFs) for multifunctional catalysis, Chem. Eur. J., 25 (2019) 10490–10498.
[36] P. Calcagnile, T. Sibillano, C. Giannini, A. Sannino, C. Demitri, Biodegradable poly(lactic acid)/cellulose-based superabsorbent hydrogel composite material as water and fertilizer reservoir in agricultural applications, J. Appl. Polym. Sci., 136 (2019) 47546, doi: 10.1002/app.47546.
[37] D.C. Montgomery, Design and Analysis of Experiments, John Wiley & Sons, USA, 2017.
[38] U. Aroke, A. Abdulkarim, R. Ogubunka, Fourier-transform infrared characterization of kaolin, granite, bentonite and barite, ATBU J. Environ. Technol., 6 (2013) 42–53.
[39] B. Davarcioğlu, E. Çİftçİ, Investigation of central anatolian clays by FTIR spectroscopy (Arapli-Yesilhisar-Kayseri, Turkey), Int. J. Nat. Eng. Sci., 3 (2009) 33154161.
[40] M.A. El-Sherbiny, G.A. El-Chaghaby, Y.M. Abd El-Shafea, Treatment of aquaculture waste effluent to be reused in fish culture in Egypt, Egypt. J. Aquat. Biol. Fish., 23 (2019) 233–243.
[41] M.M. Hamed, I. Ahmed, S. Metwally, Adsorptive removal of methylene blue as organic pollutant by marble dust as eco-friendly sorbent, J. Ind. Eng. Chem., 20 (2014) 2370–2377.
[42] S. Tamjidi, B. Kamyab Moghadas, H. Esmaeili, Ultrasound-assisted biodiesel generation from waste edible oil using $CoFe_2O_4$@GO as a superior and reclaimable nanocatalyst: optimization of two-step transesterification by RSM, Fuel, 327 (2022) 125170, doi: 10.1016/j.fuel.2022.125170.
[43] H. Khaleghi, H. Esmaeili, N. Jaafarzadeh, B. Ramavandi, Date seed activated carbon decorated with CaO and Fe_3O_4 nanoparticles as a reusable sorbent for removal of formaldehyde, Korean J. Chem. Eng., 39 (2022) 146–160.
[44] H. Khaleghi, N. Jaafarzadeh, H. Esmaeili, B. Ramavandi, Alginate@Fe_3O_4@bentonite nanocomposite for formaldehyde removal from synthetic and real effluent: optimization by central composite design, Environ. Sci. Pollut. Res., 30 (2023) 29566–29580.
[45] R.C. Barrientos, Q. Zhang, Recent advances in the mass spectrometric analysis of glycosphingolipidome–a review, Anal. Chim. Acta, 1132 (2020) 134–155.
[46] A. Azizullah, M.N.K. Khattak, P. Richter, D.-P. Häder, Water pollution in Pakistan and its impact on public health—a review, Environ. Int., 37 (2011) 479–497.
[47] R. Khurram, Z. Wang, M.F. Ehsan, α-Fe_2O_3-based nanocomposites: synthesis, characterization, and photocatalytic response towards wastewater treatment, Environ. Sci. Pollut. Res., 28 (2021) 17697–17711.
[48] C. Arab, R. El Kurdi, D. Patra, Effect of pH on the removal of anionic and cationic dyes using zinc curcumin oxide nanoparticles as adsorbent, Mater. Chem. Phys., 277 (2022) 125504, doi: 10.1016/j.matchemphys.2021.125504.
[49] A.F.F. Farias, K.F. Moura, J.K. Souza, R.O. Lima, J.D. Nascimento, A.A. Cutrim, E. Longo, A.S. Araujo, J.R. Carvalho-Filho,

A.G. Souza, Biodiesel obtained by ethylic transesterification using CuO, ZnO and CeO_2 supported on bentonite, Fuel, 160 (2015) 357–365.
[50] P. Mirzapour, B. Kamyab Moghadas, S. Tamjidi, H. Esmaeili, Activated carbon/bentonite/Fe_3O_4 nanocomposite for treatment of wastewater containing Reactive Red 198, Sep. Sci. Technol., 56 (2021) 2693–2707.
[51] V. Vimonses, S. Lei, B. Jin, C.W. Chow, C. Saint, Kinetic study and equilibrium isotherm analysis of Congo red adsorption by clay materials, J. Chem. Eng., 148 (2009) 354–364.
[52] M.H. Nasir, R. Nadeem, K. Akhtar, M.A. Hanif, A.M. Khalid, Efficacy of modified distillation sludge of rose (*Rosa centifolia*) petals for lead(II) and zinc(II) removal from aqueous solutions, J. Hazard. Mater., 147 (2007) 1006–1014.
[53] H. Albroomi, M.A. Elsayed, A. Baraka, M.K. Abdelmaged, Factors affecting the removal of a basic and an azo dye from artificial solutions by adsorption using activated carbon, J. Turk. Chem. Soc. Sect. A Chem., 2 (2015) 17–33.
[54] S. Dawood, T. Sen, Review on dye removal from its aqueous solution into alternative cost effective and non-conventional adsorbents, J. Chem. Process Eng., 1 (2014) 1–11.
[55] A. Dada, A. Olalekan, A. Olatunya, O. Dada, Langmuir, Freundlich, Temkin and Dubinin–Radushkevich isotherms studies of equilibrium sorption of Zn^{2+} unto phosphoric acid modified rice husk, IOSR J. Appl. Chem., 3 (2012) 38–45.
[56] I. Akbar, M.A. Hanif, U. Rashid, I.A. Bhatti, R.A. Khan, E.A. Kazerooni, Green nanocomposite for the adsorption of toxic dyes removal from colored waters, Coatings, 12 (2022) 1955, doi: 10.3390/coatings12121955.
[57] F. Fatma, P.L. Hariani, F. Riyanti, W. Sepriani, Desorption and re-adsorption of Procion Red MX-5B dye on alumina-activated carbon composite, Indones. J. Chem., 18 (2018) 222–228.
[58] E. Kerie, A. Alemu, Removal of Acid Yellow dye 17 from aqueous solutions using an activated bone char, Water Qual. Res. J., 57 (2022) 278–290.
[59] A. Alemu, E. Kerie, Removal of Acid Yellow 17 dye from aqueous solutions using activated water hyacinth (*Eichhornia crassipes*), Water Pract. Technol., 17 (2022) 1294–1304.
[60] J. Khan, M. Sayed, F. Ali, H.M. Khan, Removal of Acid Yellow 17 dye by Fenton oxidation process, Zeitschrift für Physikalische Chemie, 232 (2018) 507–525.
[61] M.A. Ashraf, M. Hussain, K. Mahmood, A. Wajid, M. Yusof, Y. Alias, I. Yusoff, Removal of Acid Yellow-17 dye from aqueous solution using eco-friendly biosorbent, Desal. Water Treat., 51 (2013) 4530–4545.
[62] C.-C. Wei, I.K. Pathiraja, E. Fabry, K. Schafer, N. Schimp, T.-P. Hu, L.P. Norcio, Removal of Acid Yellow 25 from aqueous solution by chitin prepared from waste snow crab legs, J. Encapsulation Adsorpt. Sci., 8 (2018) 139–155.
[63] M.A. El-Nemr, N.M. Abdelmonem, I. Ismail, S. Ragab, A. El Nemr, Removal of Acid Yellow 11 dye using novel modified biochar derived from watermelon peels, Desal. Water Treat., 203 (2020) 403–431.
[64] K. Karthikeyan, K. Jothivenkatachalam, Removal of Acid Yellow-17 dye from aqueous solution using turmeric industrial waste activated carbon, J. Environ. Nanotechnol., 3 (2014) 69–80.
[65] N. Saraei, M. Khanal, M. Tizghadam, Removing acidic yellow dye from wastewater using *Moringa peregrina*, Comput. Res. Progr. Appl. Sci. Eng., 8 (2022) 1–8.
[66] C. Patil, G. Ratnamala, S. Channamallayya, K. Belagavi, Adsorption studies for removal of Acid Yellow 17 using activated rice husk, Int. Res. J. Eng. Technol., 2 (2015) 769.
[67] S.M.F. Kabir, R. Cueto, S. Balamurugan, L.D. Romeo, J.T. Kuttruff, B.D. Marx, I.I. Negulescu, Removal of acid dyes from textile wastewaters using fish scales by absorption process, Clean Technol., 1 (2019) 311–324.
[68] A. Saha, P. Pandit, Removal of Acid Yellow 36 and Rhodamine B from single and binary systems by reverse micelles, Int. J. Chem. Technol. Res., 13 (2020) 383–393.
[69] K. Rita, Adsorption of yellow dye: Acid Yellow RR from its aqueous solution using two different samples of activated carbon by static batch method, Nat. Sci., 4 (2012) 112–115.
[70] T. Albanis, D. Hela, T. Sakellarides, T. Danis, Removal of dyes from aqueous solutions by adsorption on mixtures of fly ash and soil in batch and column techniques, Global Nest Int. J., 2 (2000) 237–244.